

# Structural Disorder of Native Horseradish Peroxidase C Probed by Resonance Raman and Low-Temperature Optical Absorption Spectroscopy

Qing Huang,<sup>†</sup> Krisztian Szigeti,<sup>‡</sup> Judit Fidy,<sup>‡</sup> and Reinhard Schweitzer-Stenner<sup>\*,†</sup>

Department of Chemistry, University of Puerto Rico, Río Piedras Campus, San Juan, PR 00931, and  
Institute of Biophysics and Radiation Biology, Semmelweis University, Puskin u. 9, Hungary H-1088

Received: September 6, 2002; In Final Form: January 16, 2003

We have measured the low-temperature absorption and the depolarization ratio dispersion of various intense resonance Raman lines of horseradish peroxidase C. The absorption spectra reveal significant splitting of the Q and charge-transfer bands whereas the Soret band solely exhibits a narrowing of the band profile. The depolarization ratios of all Raman lines investigated are different from expectation values in  $D_{4h}$  symmetry and show significant dispersion in the preresonance and resonance region of the  $Q_v$  band. All these data indicate symmetry lowering distortions of the heme macrocycle. An analysis of the depolarization ratios shows that in-plane  $B_{1g}$ - and  $B_{2g}$ -type perturbations distort the heme along the N–Fe–N and  $C_m$ –Fe– $C_m$  line of the heme. The  $B_{1g}$  perturbation gives rise to the band splitting in the optical spectrum and to a rhombicity of the iron's ligand field detected by EPR experiments. On the basis of group theoretical arguments we propose that particularly the strong  $B_{2g}$  distortion gives rise to the quantum mixed spin state characteristic of class III peroxidases.

## Introduction

Peroxidases are enzymes participating in a large variety of oxidation and reduction process. Owing to its essential functions, stability, and availability, the class III protein horseradish peroxidase C (HRPC) is the most intensively studied peroxidase. It serves as the model system for exploring the underlying mechanisms of the structure–function relationship of peroxidases.<sup>1</sup> It is a monomeric protein with thirteen  $\alpha$ -helices and two antiparallel  $\beta$ -strands. The structural details of the substrate oxidation process are well-known and described elsewhere.<sup>1</sup> The structure of the distal heme pocket has a major impact on the enzymatic reactivity. This particularly concerns the position of His 42, Arg 38, Phe 41 (Figure 1), and a scaffolding H-bond network between these residues, the substrate and the axial ligands of the transition states.<sup>2–5</sup> With respect to the proximal side, His 170 is generally thought to control the reduction potential of the heme iron. In HRP, His 170 is H-bonded to Asp 247. This is assumed to increase the negative charge on the His ligand and thus stabilizes the low reduction potential.<sup>1</sup>

Although the role of the distal site in controlling the different steps of the enzymatic reactions is well established, our knowledge on how the ligand field of the heme iron provided by the proximal imidazole and the heme nitrogens affect processes such as ligand binding and iron/porphyrin oxidation is still limited. With respect to the heme group, strong evidence has been provided that symmetry-lowering deformations affect spin delocalization, redox potential, the electronic structure and the vibrational dynamics of the macrocycle<sup>6</sup> as well as the affinity and the geometry of axial ligand binding.<sup>7,8</sup> In this

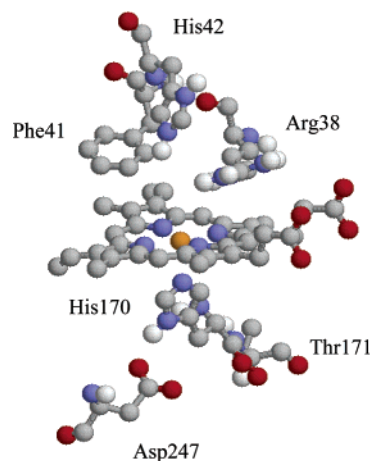


**Figure 1.** Crystallographic structure of HRPC–BHA. The substrate complex has been omitted. The structure was reported by Gajhede et al.<sup>46</sup> and downloaded from the Protein Data Bank.

context, a strong emphasis has been put on nonplanar distortions (i.e., ruffling, saddling, and doming), which are particularly prominent in various cytochrome *c* derivatives, but heme nonplanarity is also detectable in various derivatives of myoglobin and hemoglobin.<sup>8–10</sup> Recently, Howes et al.<sup>11</sup> reported the result of a normal coordinate deformation (NCD) analysis of several peroxidases. They identified significant saddling and ruffling in nearly all of the investigated proteins. Though nonplanar distortions have attracted considerable attention, the number of studies dealing with in-plane distortions induced by asymmetrically arranged peripheral substituents and chromophore–protein interactions are rather limited, even though ample evidence was provided that they can significantly affect ligand binding properties.<sup>7</sup> This results from the fact that their determination from crystal structures is subject to relatively large statistical errors (J.A. Shelnut, private communication). With

\* Corresponding author: Reinhard Schweitzer-Stenner, Department of Chemistry, University of Puerto Rico, Río Piedras Campus, P.O. Box 23346, Facundo Bueso Bldg. FB110, San Juan, PR 00931. Phone: 1-787-764-0000, Ext 2417. Fax: 1-787-756-8242. E-mail: rstenner\_upr\_chemistry@gmx.net.

<sup>†</sup> University of Puerto Rico.

<sup>‡</sup> Semmelweis University.

respect to HRP, fluorescence and absorption measurements have revealed a splitting of the Q band at low temperatures for HRP–CO, HRP–CO complexed with benzohydroxamic acid (BHA),<sup>12,13</sup> and Mg-mesoporphyrin-IX substituted HRP.<sup>14,15</sup> However, a detailed analysis and characterization of the distortions giving rise to the observed band splitting is outstanding.

In the present study we combine optical and resonance Raman spectroscopy with group theory to analyze distortions in native HRP C. First, we perform absorption measurements at low temperatures to identify possible splitting of the absorption band. Second, we use polarized resonance Raman dispersion spectroscopy (PRRDS) to probe static normal coordinate deformations (SNCD) of the heme group at different pHs.<sup>16</sup> Our results lead us to conclude that the heme macrocycle is subject to significant rhombic distortions along the N–Fe–N axis and to triclinic distortions that affect the position of the methin carbons as well as the internal symmetry of the pyrrole rings.

### Theoretical Background of PRDS

Details of theory used to analyze the depolarization ratio dispersion and the resonance excitation profiles of porphyrin Raman lines have been published elsewhere.<sup>16</sup> In this paper we confine ourselves to a brief, more qualitative discussion of the relationship between DPD and SNCD.

**Porphyrins in  $D_{4h}$  Symmetry.** In the ideal case of identical  $C_m$  and  $C_\beta$  substituents a porphyrin macrocycle exhibits a planar conformation of  $D_{4h}$  symmetry. In this case the two lowest excited states Q and B are 2-fold degenerate and exhibit  $E_u$  symmetry. As a consequence, only  $A_{1g}^-$ ,  $B_{1g}^-$ ,  $B_{2g}^-$ , and  $A_{2g}^-$  type modes are resonance Raman active with B- and Q-band excitation. Following McClain,<sup>17</sup> their respective tensors can be written as

$$\alpha^{A_{1g}^-} = \begin{pmatrix} a_{1g}(\tilde{\nu}_L) & 0 \\ 0 & a_{1g}(\tilde{\nu}_L) \end{pmatrix} \quad \alpha^{B_{1g}^-} = \begin{pmatrix} b_{1g}(\tilde{\nu}_L) & 0 \\ 0 & -b_{1g}(\tilde{\nu}_L) \end{pmatrix}$$

$$\alpha^{A_{2g}^-} = \begin{pmatrix} 0 & a_{2g}(\tilde{\nu}_L) \\ -a_{2g}(\tilde{\nu}_L) & 0 \end{pmatrix} \quad \alpha^{B_{2g}^-} = \begin{pmatrix} 0 & b_{2g}(\tilde{\nu}_L) \\ -b_{2g}(\tilde{\nu}_L) & 0 \end{pmatrix} \quad (1)$$

The tensor elements  $\Gamma(\tilde{\nu}_L)$  depend on transition dipole moments, the vibronic coupling operators of the respective Raman mode, and specific frequency functions related to the contributing vibronic coupling processes.<sup>16,20</sup> Because no transitions polarized perpendicular to the molecular plane are of relevance for Raman scattering of in-plane modes for porphyrins in ideal  $D_{4h}$ , all  $z$ -components of the Raman tensor  $\hat{\alpha}$  are zero. The tensor elements are calculated as the coherent superposition of all scattering amplitudes brought about by Franck–Condon, Herzberg–Teller, and Jahn–Teller coupling within and between the above-mentioned excited states.<sup>16</sup> Though the tensor elements are functions of the excitation wavenumber  $\tilde{\nu}_L$ , the depolarization ratios of all Raman lines are frequency independent, namely  $\rho = 0.125$  for  $A_{1g}^-$ , 0.75 for  $B_{1g}^-$  and  $B_{2g}^-$  modes, and  $\infty$  for  $A_{2g}^-$  modes. An example for a porphyrin with perfect  $D_{4h}$  symmetry is Ni(II)–porphin.<sup>18</sup>

**Asymmetric Distortions of the Porphyrin Macrocycle.** Peripheral substituents or interactions with a protein matrix give rise to symmetry lowering distortions  $\Delta$  of the porphyrin macrocycle, which can be described as a superposition of SNCDs  $\delta\bar{Q}_i^{\Gamma_i}$ .<sup>8</sup>

$$\Delta = \sum_{\Gamma_i, i} \gamma_i^{\Gamma_i} \delta\bar{Q}_i^{\Gamma_i} \quad (2)$$

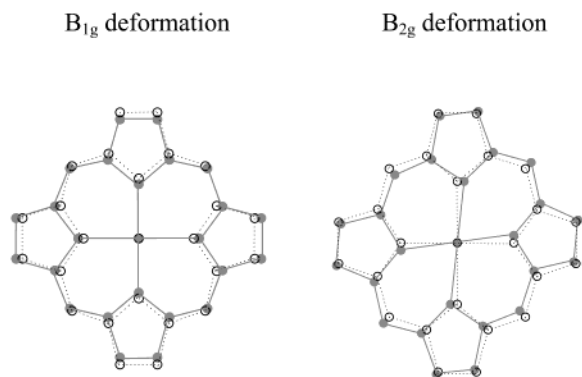


**Figure 2.** Planar deformations of the heme macrocycle along the normal coordinates of the lowest energy  $B_{1g}$  and  $B_{2g}$  modes as used in the NSD analysis of heme groups and porphyrins as obtained from J. A. Shelnett, <http://jasheln.unm.edu>.<sup>41</sup>

where  $\gamma_i^{\Gamma_i}$  denotes the amplitude of the distortion along the normal coordinate of the  $i$ th vibration of  $D_{4h}$  symmetry  $\Gamma_i$ . As shown in recent analyses of isolated porphyrins and heme groups in various proteins,  $\Delta$  is dominated by the normal coordinates of the lowest frequency modes of the respective symmetry representations.<sup>8</sup> Figure 2 exhibits representations of the  $B_{1g}$  and  $B_{2g}$  distortions along the normal coordinates of the respective lowest frequency modes  $\nu_{18}$  and  $\nu_{35}$  obtained for the model substance Ni(II)–octaethylporphyrin.<sup>19</sup>  $\nu_{18}$  ( $B_{1g}$ ) is a rhombic distortion along the orthogonal N–Fe–N lines, involving expansion and contraction of Fe–N distances.  $\nu_{35}$  ( $B_{2g}$ ) is a triclinic distortion that affects the Fe– $C_m$  distances and the internal pyrrole symmetry. It destroys the orthogonal orientation of the two N–Fe–N lines.

To account for the above symmetry lowering distortions, we expand the vibronic coupling operator of the mode  $\bar{Q}_r^{\Gamma_r}$  ( $\bar{\Gamma}_r$  is now the representation in the lower symmetry group) into a Taylor series in second order:

$$\frac{\partial \hat{H}_{el}(q, Q)}{\partial \bar{Q}_r^{\Gamma_r}} = \frac{\partial \hat{H}_{el0}(q, Q)}{\partial \bar{Q}_r^{\Gamma_r}} + \sum_{\Gamma_i, i} \sum \frac{\partial^2 \hat{H}_{el0}(q, Q)}{\partial \bar{Q}_r^{\Gamma_r} \partial \bar{Q}_i^{\Gamma_i}} \delta \bar{Q}_i^{\Gamma_i} +$$

$$\sum_{\Gamma_i, \Gamma_j, i, j} \frac{\partial^3 \hat{H}_{el0}(q, Q)}{\partial \bar{Q}_r^{\Gamma_r} \partial \bar{Q}_i^{\Gamma_i} \partial \bar{Q}_j^{\Gamma_j}} \delta \bar{Q}_i^{\Gamma_i} \delta \bar{Q}_j^{\Gamma_j} \quad (3)$$

To couple electronic states of  $E_u$  symmetry, the representation  $\bar{\Gamma}_r$  of the vibronic operators in eq 3 must transform like  $A_{1g}$ ,  $B_{1g}$ ,  $B_{2g}$ , or  $A_{2g}$ . This requirement is met by the first-order term, if the product  $\bar{\Gamma}_r = \Gamma_r \otimes \Gamma_i$  contains at least one of these four representations. It is met by the second-order term, if this condition also holds for the product  $\bar{\Gamma}_r = \Gamma_r \otimes \Gamma_i \otimes \Gamma_j$ . Hence, the contribution  $\bar{\Gamma}_r$  of the first and second-order term in eq 3 to the vibronic coupling operator must transform like the representation  $\bar{\Gamma}_r$  of the observed Raman mode multiplied with the representations  $\Gamma_i$  and  $\Gamma_j$  of the SNCDs. As an example, a distortion of  $\Gamma_i = B_{2g}$  symmetry gives rise to a first-order contribution by admixing a  $\bar{\Gamma}_r = A_{2g}$  symmetry tensor into the Raman tensor of a mode having  $\bar{\Gamma}_r = B_{1g}$  symmetry in  $D_{4h}$ , so that the effective symmetry  $\bar{\Gamma}_r$  reads as  $B_{1g} + A_{2g}$ .

Thus, in the most general case of a sufficiently low symmetry, admixtures of  $A_{1g}$ ,  $B_{1g}$ ,  $B_{2g}$  and  $A_{2g}$  tensors occur. As a consequence, the Raman tensor of the representation  $\bar{\Gamma}_r$  can be expressed as a linear combination of the  $D_{4h}$ -tensors in eq 3, so that in the lower symmetry:<sup>20</sup>

$$\hat{\alpha} = \begin{bmatrix} a_{1g}(\tilde{\nu}_L) + b_{1g}(\tilde{\nu}_L) & b_{2g}(\tilde{\nu}_L) + a_{2g}(\tilde{\nu}_L) \\ b_{1g}(\tilde{\nu}_L) + a_{2g}(\tilde{\nu}_L) & a_{1g}(\tilde{\nu}_L) - b_{1g}(\tilde{\nu}_L) \end{bmatrix} \quad (4)$$

By using the invariants of the isotropic, anisotropic and antisymmetric part of the Raman tensor the DPR can be calculated to<sup>20</sup>

$$\rho = \frac{3}{4} \frac{a_{1g}^2(\tilde{\nu}_L) + 5a_{2g}^2(\tilde{\nu}_L) + 2(b_{1g}^2(\tilde{\nu}_L) + b_{2g}^2(\tilde{\nu}_L))}{6a_{1g}^2(\tilde{\nu}_L) + 2(b_{1g}^2(\tilde{\nu}_L) + b_{2g}^2(\tilde{\nu}_L))} \quad (5)$$

Equation 5 shows that  $\rho$  becomes independent of  $\tilde{\nu}_L$ , if only one symmetry type is present and the Raman tensor is represented by one of the forms in eq 1. This is the case in  $D_{4h}$ , but also in  $D_{4d}$ ,  $D_4$ ,  $C_{4v}$ , and  $D_{2d}$ . As can be seen by group correlation tables, mixing of the  $D_{4h}$  representations  $A_{1g}$ ,  $B_{1g}$ ,  $B_{2g}$ , and  $A_{2g}$  occur for all point groups with symmetries lower than these, e.g.,  $S_4$ ,  $C_4$ ,  $C_{2h}$ ,  $D_2$ ,  $C_{2v}$ . As a consequence, one obtains a dispersion of the DPR, because  $a_{1g}^2(\tilde{\nu}_L)$ ,  $a_{2g}^2(\tilde{\nu}_L)$ ,  $b_{1g}^2(\tilde{\nu}_L)$ , and  $b_{2g}^2(\tilde{\nu}_L)$  depend differently on the excitation frequency.<sup>16,20</sup>

**Simulation of DPR Dispersion.** We performed some theoretical simulations to illustrate how asymmetric distortions affect the depolarization ratios of some prominent Raman modes of metalloporphyrins. For the sake of simplicity we used only the first-order term of the Raman tensor reported by Unger et al.,<sup>18</sup> thus neglecting multimode mixing. Because we consider asymmetrically distorted porphyrins, the Raman tensor was expressed as a linear combination of McClain tensors for  $A_{1g}$ ,  $B_{1g}$ ,  $A_{2g}$ , and  $B_{2g}$  modes, as described above. To describe the degree of symmetry mixing for the performed simulations, we introduce sets of normalized symmetry mixing factors  $f_{\Gamma}$ , i.e.,  $(f_{A_{1g}}, f_{B_{1g}}, f_{A_{2g}}, f_{B_{2g}})$ . For undistorted  $A_{1g}$ ,  $B_{1g}$ ,  $A_{2g}$ , or  $B_{2g}$  modes in  $D_{4h}$ ,  $(f_{A_{1g}}, f_{B_{1g}}, f_{A_{2g}}, f_{B_{2g}}) = (\mathbf{1}, 0, 0, 0)$ ,  $(0, \mathbf{1}, 0, 0)$ ,  $(0, 0, \mathbf{1}, 0)$ , or  $(0, 0, 0, \mathbf{1})$ , respectively. The admixture of other symmetries due to symmetry lowering distortions is then reflected by the respective factors  $f_{\Gamma}$  in the set.  $(f_{A_{1g}}, f_{B_{1g}}, f_{A_{2g}}, f_{B_{2g}}) = (0.1, \mathbf{1}, 0, 0)$ , for example, represents an  $A_{1g}$  admixture to the Raman tensor of a  $B_{1g}$  mode (marked by a bold number), which, due to eq 3, results either from an in-plane  $B_{1g}$  distortion or from the combination of two out-of-plane distortions ( $A_{1u}$  and  $B_{1u}$  or  $A_{2u}$  or  $B_{2u}$ ). The energies of the involved vibronic states, the transition dipole moments associated with the transitions into the Q and B states, and the respective Lorentzian bandwidths were estimated from the optical spectrum and listed in Table 1. It contains also the values for the coupling parameters  $C_{lm}^{\Gamma}$  used for the simulation, i.e., the matrix elements of the vibronic coupling operator defined by eq 3 in the basis of the excited electronic states  $Q_x$ ,  $Q_y$ ,  $B_x$ , and  $B_y$  of the unperturbed heme (electronic distortions are thus neglected). The interested reader can refer to ref 16 for more details. These  $C_{lm}^{\Gamma}$  values are on the order of magnitude of parameters obtained from the resonance excitation profiles and depolarization ratios of various porphyrins.<sup>16</sup> The factors  $f_{\Gamma}$  are linear scaling factors of these parameters, the values in Table 1 represent the coupling strength for  $f_{\Gamma} = 1$ .

Figure 3 illustrates how  $B_{1g}$  and  $B_{2g}$  distortions affect the depolarization ratios of modes exhibiting  $A_{1g}$  (2a),  $A_{2g}$  (2b), and  $B_{1g}$  (2c) symmetry in  $D_{4h}$ . The calculations were performed for the wavenumber region between 23 000 and 19 000  $\text{cm}^{-1}$ , which can be explored by the excitation wavelengths of our argon ion laser. It thus covers the resonance and preresonance region of the  $Q_v$  band. Different dispersion curves for a particular mode reflect different degrees of symmetry mixing. Figure 3a shows the DPRs for an  $A_{1g}$ -type mode. The DPR of the unperturbed

mode is 0.125.  $B_{1g}$  and  $B_{2g}$  distortions admix  $B_{1g}$  and  $B_{2g}$  symmetries ( $f_{B_{1g}}, f_{B_{2g}} \neq 0$ ) to this mode, respectively. Larger symmetry-mixing factors represent larger distortions. The DPR generally increases toward the resonance position of the  $Q_v$  band due to an increasing contribution from  $B_{1g}$ - and  $B_{2g}$ -type Herzberg–Teller coupling.<sup>16</sup> Figure 3b exhibits the DPR dispersion for an  $A_{2g}$  mode. Now,  $B_{1g}$  and  $B_{2g}$  distortions admix  $B_{2g}$ - and  $B_{1g}$ -type contributions to its Raman tensor. As expected, the simulation shows that the considered distortions cause the DPR to vary between infinite and 0.75. For increasing distortions, the DPR is shifted closer to 0.75. Finally, Figure 3c depicts DPR simulations for a  $B_{1g}$ -type Raman mode. The simulations show that the DPRs do not deviate much from the expectation value of 0.75. It is noteworthy that  $B_{1g}$  distortion admixes  $A_{1g}$  symmetry ( $f_{A_{1g}} \neq 0$ ) so that it causes DPRs smaller than 0.75, whereas  $B_{2g}$  distortion admixes  $A_{2g}$  symmetry to give rise to DPRs larger than 0.75 ( $f_{A_{2g}} \neq 0$ ). Therefore, we can utilize the experimentally observed DPRs of  $B_{1g}$  modes to distinguish between  $B_{1g}$  and  $B_{2g}$  distortions, which cannot be done on the basis of the DPRs of  $A_{1g}$  and  $A_{2g}$  modes.

A comment on our use of terminology is at place in this context. In what follows we distinguish between distortions and perturbations. Distortions are described by eq 2. Perturbations can be subdivided into electronic and vibronic perturbations.<sup>21</sup> Electronic perturbations can be described as the derivative of the pure electronic Hamiltonian with respect to considered distortional coordinate. Vibronic perturbations are described by the third and second term in eq 3. Although an electronic perturbation exhibits always the symmetry of the related distortion, this is not necessarily the case for vibronic distortions, as described above.

## Material and Methods

**Sample Preparation.** Horseradish isoenzyme C as salt-free lyophilized powder (code HRP4B) was purchased from Biozyme Laboratories Ltd. Because of its high *Reinheitszahl* (3.4) and high percentage (90%) of isoenzyme C, our aqueous solution samples were prepared without further purification. For Raman measurements, HRPC was dissolved in either Tris buffer (pH 8) or phosphate buffer (pH 5), and a concentration of 1 mM was used.

**Low-Temperature Absorption Measurements.** For the low- $T$  absorption measurements, HRPC was applied to a G-75 column (Sephadex Superfine, Pharmacia Fine Chemicals, Uppsala, Sweden), degassed after swelling, bed volume: 76 mL) equilibrated in 50 mM Tris/HCl, pH 8, and eluted at a rate of 1 mL  $\text{h}^{-1}$ . Only the main band fractions with  $RZ > 3.5$  were retained. The spectra were recorded using  $\sim 30 \mu\text{M}$  samples in 50% glycerol/buffer, which ensures good optical quality at cryogenic temperatures. The samples were placed in a sample holder with 0.5 mm path length, and the measurements were performed using a CTI-Cryogenics Model 22 refrigeration unit (Cryophysics SA, Geneva) inserted in the cavity of a double beam Varian Cary 4 UV–vis instrument with wavelength accuracy of  $\pm 0.1$  nm.

**Resonance Raman Spectroscopy.** Raman spectra were obtained in a  $135^\circ$  backscattering geometry by excitation with eight radiation lines from a tunable argon ion laser (Lexel 95). The excitation ranges from 457.9 to 514.5 nm, thus covering the resonant region of the Q band of HRP. Interference filters were used to eliminate useless plasma light in the output laser beam before the beam was focused on the solution sample in a quartz cell. Typically, a laser power was chosen below 20 mW to avoid heating of the sample. The scattered light was collected

**TABLE 1: Parameters Used for the Simulation of Depolarization Dispersion Curves**

parameter description	parameter notation	parameter value
energy $Q_0$	$E_{Q_0}$	19874 cm <sup>-1</sup>
energy $B_0$	$E_{B_0}$	26400 cm <sup>-1</sup>
Lorentzian half-width Q band	$\Gamma_Q$	650 cm <sup>-1</sup>
Lorentzian half-width B band	$\Gamma_B$	750 cm <sup>-1</sup>
ratio of dipole strengths	$R_Q/R_B$	0.05
A <sub>1g</sub> , Franck–Condon coupling Q state	$C_{QQ}^{A_{1g}}$	150 cm <sup>-1</sup>
A <sub>1g</sub> , Franck–Condon coupling B state	$C_{BB}^{A_{1g}}$	50 cm <sup>-1</sup>
A <sub>1g</sub> , Herzberg–Teller coupling between Q and B states	$C_{QB}^{A_{1g}}$	-50 cm <sup>-1</sup>
B <sub>1g</sub> , Jahn–Teller coupling Q and B states	$C_{QQ}^{B_{1g}} = -C_{BB}^{B_{1g}}$	200 cm <sup>-1</sup>
B <sub>1g</sub> , Herzberg–Teller coupling between Q and B states	$C_{QB}^{B_{1g}}$	-250 cm <sup>-1</sup>
B <sub>2g</sub> , Jahn–Teller coupling Q and B states	$C_{QQ}^{B_{2g}} = -C_{BB}^{B_{2g}}$	150 cm <sup>-1</sup>
B <sub>2g</sub> , Herzberg–Teller coupling between Q and B states	$C_{QB}^{B_{2g}}$	-150 cm <sup>-1</sup>
A <sub>2g</sub> , Herzberg–Teller coupling between Q and B states	$C_{QB}^{A_{2g}}$	400 cm <sup>-1</sup>

**TABLE 2: Normal-Coordinate Structure Decomposition (NSD) Result of Native HRPC Generated from File 1Atj\_c.pdb (unit: Å)**

basis	Dip	dip	B <sub>2g</sub>	B <sub>1g</sub>	$E_u(x)$	$E_u(y)$	A <sub>1g</sub>	A <sub>2g</sub>
min	0.3677	0.0411	-0.3056	0.1832	-0.0728	-0.0351	0.0411	-0.0098
ext	0.4102	0.0212	-0.3034	0.1834	-0.0726	-0.0361	0.0373	-0.0096
			0.1423	-0.0119	-0.0230	-0.0731	-0.0518	0.0640
			-0.0004	0.0107	0.0381	0.0368	-0.0550	-0.0188
			0.0071	-0.0007	-0.0234	0.0268	0.0171	0.0096
			0.0141	0.0016	-0.0133	-0.0154	-0.0290	0.0136
			0.0232	0.0029	0.0357	-0.0368	-0.0199	
					-0.0144	-0.0141		
					0.0119	0.0088		
					-0.0012	0.0022		
					0.0062	0.0093		
					-0.0014	-0.0073		
comp	0.4267	0.0000	0.3381	0.1839	0.0984	0.1035	0.0931	0.0696
basis	Doop	doop	B <sub>2u</sub>	B <sub>1u</sub>	A <sub>2u</sub>	$E_g(x)$	$E_g(y)$	A <sub>1u</sub>
min	0.9131	0.0149	-0.8712	-0.0845	-0.0673	-0.1407	-0.2079	-0.0017
ext	0.9150	0.0099	-0.8710	-0.0845	-0.0686	-0.1388	-0.2072	-0.0017
			0.0197	0.0233	-0.0097	0.0457	0.0142	0.0177
			-0.0120	0.0032	-0.0208	0.0275	-0.0194	
						-0.0221	0.0309	
						0.0028	0.0052	
comp	0.9168	0.0000	0.8715	0.0877	0.0710	0.1520	0.2116	0.0178

and focused into an entrance slit of 100 μm width of a triple-grating spectrometer (Jobin-Yvon T64000). Polarized spectra were obtained by utilizing a polaroid analyzer that was inserted between the sample and the entrance slit of the spectrometer. To correctly record the intensity of scattered light, which is polarized in the direction of either perpendicular ( $I_y$ ) or parallel ( $I_x$ ) to the polarization of the incident laser beam, an optical scrambler was inserted between the polaroid analyzer and spectrometer because it can effectively smooth away the polarization sensitivity of the gratings of the spectrometer. After dispersed by the gratings, the scattered light was finally detected by a liquid nitrogen cooled CCD camera (CCD3000 from Jobin-Ivon) with a 1024 × 512 pixel array chip. A Dell computer with Pentium III processor controls all the operations of the spectrometer, CCD, and data processing. The spectrometer was calibrated by using the Raman line at 934 cm<sup>-1</sup> of ClO<sub>4</sub><sup>-</sup>. The recorded Raman spectra have an accuracy of 1 cm<sup>-1</sup>.

**Spectral Analysis.** All spectra were analyzed by the program MULTIFIT, which was developed in the Optical Spectroscopy Group at the Institute of Experimental Physics of the University of Bremen, Bremen, Germany.<sup>22</sup> This program greatly facilitates the fitting procedure in that it can not only fit many overlapping bands simultaneously but also takes into account the spectral convolution of the natural profile of each Raman band with the profile of spectrometer slit function. We found that it is a

Gaussian profile of the spectrometer slit function that convolutes with the Raman signal, leading to a Voigtian profile for each Raman band. To achieve a more reliable spectral analysis, all spectra were decomposed consistently by using the same parameters such as half-width, frequency position, and band profile for all eight excitation wavelengths, and the best fitting parameters were obtained by checking the smallest  $\chi^2$  values for statistical errors. The intensities of the polarized bands were derived from their band areas. The depolarization ratios  $\rho$  of thus identified spectral lines were calculated as

$$\rho = \frac{I_y}{I_x} \quad (6)$$

where  $I_x$  and  $I_y$  were measured parallel and perpendicular to the polarization of the exciting laser beam. The accuracy of the depolarization ratio was checked with the 216 cm<sup>-1</sup> line of CCl<sub>4</sub>. The measured depolarization ratio was found to be identical with its expectation value of 0.75 ± 0.02 at all excitation wavelengths. Moreover, the depolarization ratio of the 934 cm<sup>-1</sup> line of the internal standard ClO<sub>4</sub><sup>-</sup> was always close to 0, as theoretically expected. This shows that the contamination by the collimator optics is negligibly small for polarized and depolarized lines.

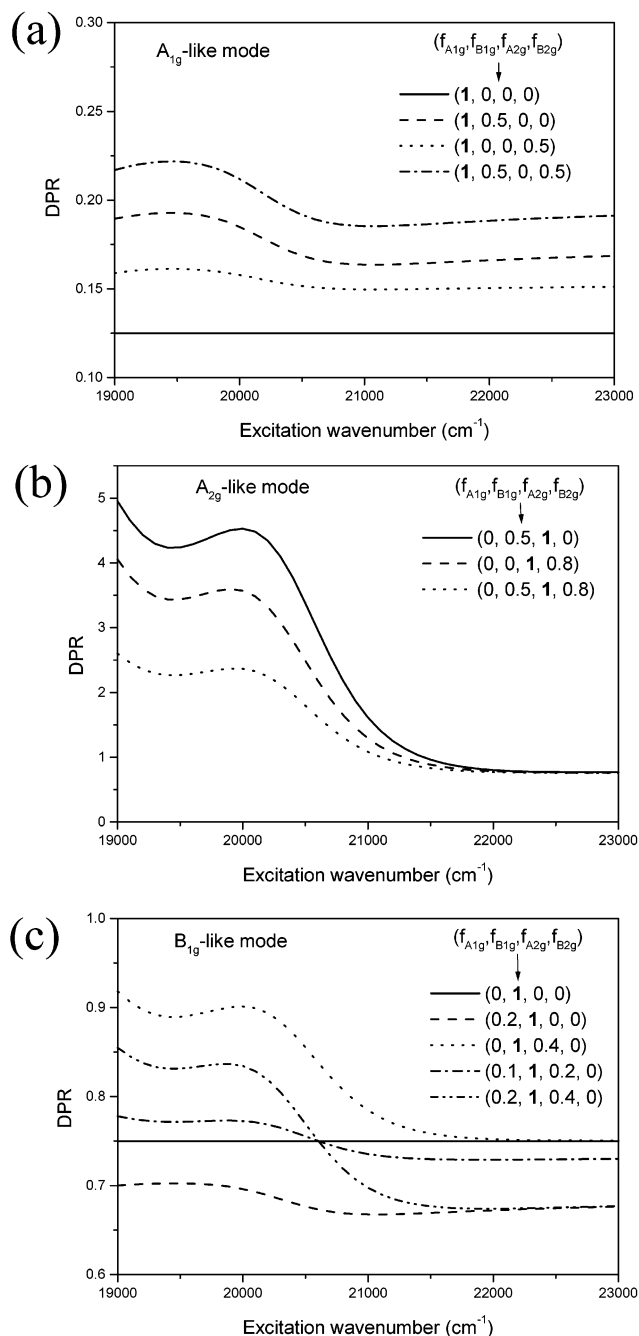


**Figure 3.** Simulation of the dispersion of the depolarization ratio for (a)  $\nu_4$ , (b)  $\nu_{21}$ , and (c)  $\nu_{11}$  of HRPC in the resonance and pre-resonance region of the  $Q_v$  band. Details are described in the text.

## Results and Discussion

**Absorption Spectra.** Figures 4 and 5 show the B-band and Q-band regions of the optical absorption spectrum of HRP C in a water/glycerol mixture recorded at different temperatures between 9 and 150 K. All these temperatures are below the glass transition temperature of the solvent. The Soret band at 404 nm (Figure 4) is hardly shifting but narrows substantially upon temperature lowering. It appears only slightly blue shifted with respect to its room-temperature position. The sideband at 383 nm becomes more pronounced in the lowest temperature spectra due to line narrowing. In his recent book on heme peroxidases Dunford<sup>23</sup> described the appearance of the band at 380 nm (in the room-temperature spectrum) as a yet unexplained mystery. However, there is no mystery at all with this band, because it is clearly assignable to the vibronic sideband  $B_v$ . The

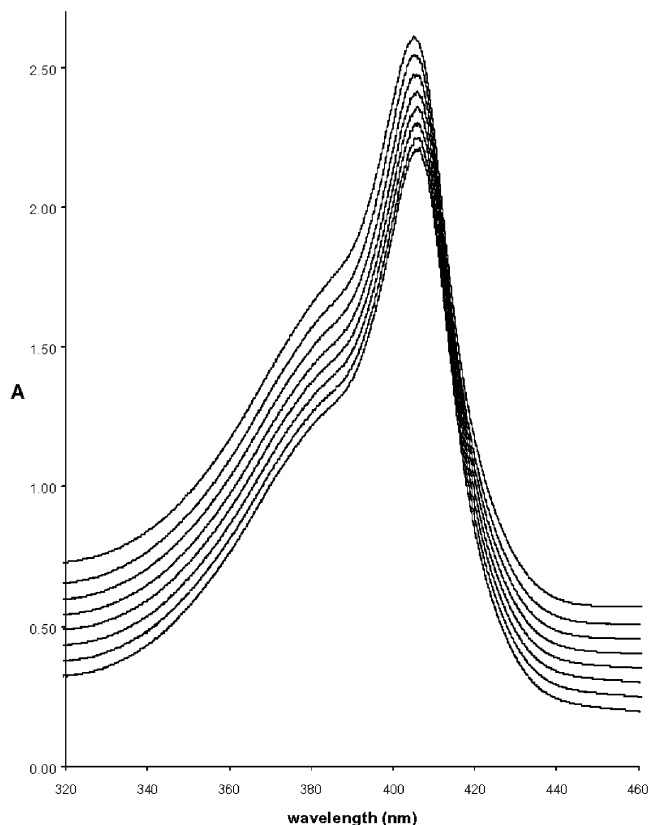


**Figure 4.** Temperature dependence of the absorption in the Soret band region of HRPC (concentration:  $\sim 100 \mu\text{M}$  native HRPC in 10 mM Tris/HCl and 50% glycerol v/v, pH 8). The temperature in Kelvin from bottom to top is 8.7, 17.8, 29.6, 39.6, 49.3, 69, 99, and 149.

wavenumber difference between  $B_v$  and  $B_0$  is  $1360 \text{ cm}^{-1}$ , which is very close to the ground state frequency of the  $\nu_4$  mode, which, owing to its strong relative intensity, is expected to account for most of the vibronic coupling in the high-frequency region.<sup>24</sup> The  $B_0$  band particularly in the 9 K spectrum appears pretty narrow and symmetric and does not indicate any substantial band splitting. The Q-band region (Figure 5) displays three bands at 500, 535, and 640 nm. The latter is generally assigned to a charge-transfer transition (CT) from an  $a_{2u}$  HOMO of the heme to the  $d_{xy}/d_{yz}$  orbital, which is double degenerate in a crystal field of tetragonal symmetry concomitant with a  $D_{4h}$  heme symmetry.<sup>25</sup> The assignment of the 495 nm band is controversial. On the basis of the very detailed polarized absorption measurement on single crystals, Eaton and Hochstrasser assigned the corresponding band in the spectrum of high spin metmyoglobin species to  $Q_v$ .<sup>25</sup> In this case the shoulder at 535 nm is assignable to  $Q_0$ . On the contrary, Dunford<sup>23</sup> assigned it to a charge-transfer bands  $CT_2$  from a lower lying porphyrin orbital to  $d_{xy}/d_{yz}$  (Fe) and attributed the weak and broad band at 530 nm (535 nm in our low-temperature spectra) to  $Q_v$ . For  $Q_0$ , he invoked a hardly detectable band at 580 nm. This interpretation is highly unlikely to be correct for physical reasons. It is well established that nearly 80% of the  $Q_v$ -band intensity stems from vibronic Herzberg–Teller coupling between Q and B states.<sup>18</sup> Its intensity is proportional to the oscillator strength of the B band and to the square of the vibronic coupling energy of the involved heme vibrations.<sup>18</sup> As a consequence  $Q_v$  has significant oscillator strength even if the transition dipole moment for the Q band is very weak, as observed for meso-substituted metalloporphyrins in solution.<sup>26</sup> Thus, it is highly unlikely that the  $Q_v$  band shows less intensity than a charge-transfer band. Moreover, Dunford's assignment

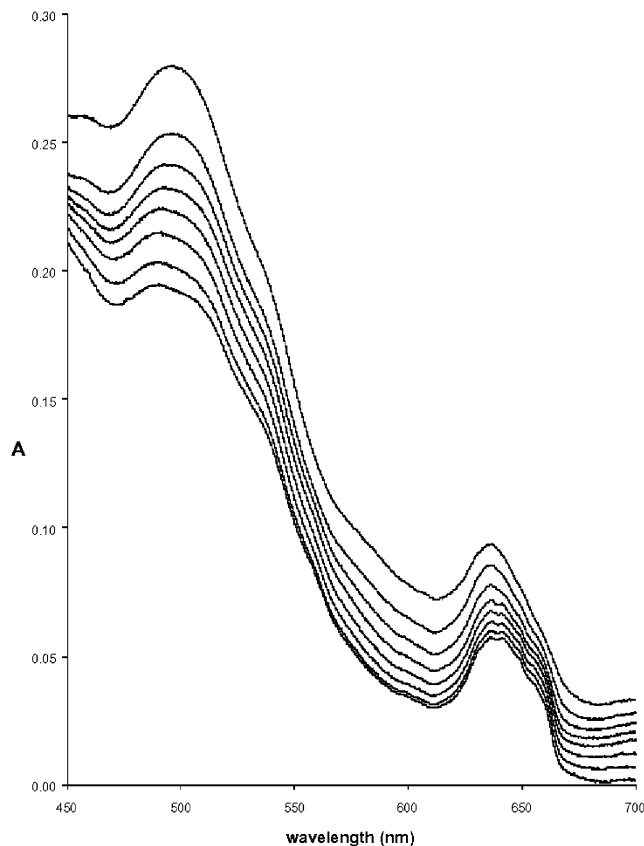


**Figure 5.** Temperature dependence of the absorption in Q-band/CT region of HRP C (concentration: 100  $\mu$ M native HRP C in 10 mM Tris/HCl and 50% glycerol v/v, pH 8). The temperature in Kelvin from bottom to top is 8.7, 17.8, 29.6, 39.6, 49.3, 69, 99, and 149.

implies a wavenumber difference of ca. 1630  $\text{cm}^{-1}$  between  $Q_0$  and  $Q_v$ , which is significantly larger than the generally obtained differences between 1200 and 1300  $\text{cm}^{-1}$ .<sup>16,18</sup> However, if one follows Eaton and Hochstrasser<sup>25</sup> in assigning the 500 and 535 nm band to a  $Q_v/Q$  pair, respectively, one obtains a difference of 1300  $\text{cm}^{-1}$ , apparently a much more reasonable value. In an earlier study, Smulevich et al.<sup>27</sup> suggested something like a compromise by invoking the possibility that the 500 nm band is mostly  $Q_v$ , but with some underlying charge-transfer contribution. We think that the most reasonable interpretation had much earlier been suggested by Zerner et al.,<sup>28</sup> i.e., an electronic mixing between CT and Q states. In fact this has been experimentally proven by Asher et al.<sup>29</sup> for the ferric high spin hemoglobin fluoride ( $\text{HBF}^-$ ) in that they obtained a resonance enhancement of  $B_{1g}^-$  and  $A_{2g}^-$ -type Raman modes of the heme upon excitation in the CT-band region (600 nm in their spectrum).

Interestingly, further evidence for the above electronic coupling can be deduced from our low-temperature experiments. The spectra taken at 9 K clearly reveals a band splitting of the 640 (ca. 450  $\text{cm}^{-1}$ ) and also of the 500 nm band (ca. 280  $\text{cm}^{-1}$ ). This results from lifting the degeneracy of the involved excited states by symmetry lowering perturbations of the heme macrocycle. The  $Q_v$ -band splitting is a result of the  $Q_0$ -splitting and additional vibronic contributions particularly from  $\nu_{19}$ .<sup>30</sup> In addition, the two components of the CT band at 640 nm exhibit different intensities. This strongly indicates to  $A_{1g}^-$  and  $B_{1g}^-$ -type electronic coupling between the CT state and the higher lying Q state, because the respective intrastate coupling of the CT state can only lift the degeneracy but has no influence on the intensity distribution.<sup>30</sup>

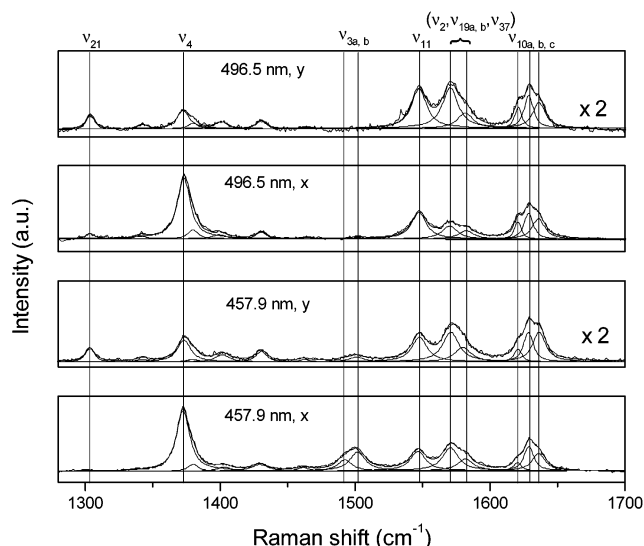


**Figure 6.** Raman spectra of native HRP C (pH 8) recorded with 457.9 and 496.5 nm excitation.

At first sight it might be surprising that only the Q (and also the CT band) exhibits significant splitting, whereas it is not detectable for the B bands. However, the different splitting of Q and B bands in the presence of symmetry lowering perturbations is a well established phenomenon that can be observed even in highly distorted heme porphyrins. Recently, it was shown by Schweitzer-Stenner and Bigman<sup>30</sup> that this results from an interference between electronic and vibronic perturbations, which depends on the sign of the coupling parameters, so that contributions can add up for the Q state, whereas they nearly cancel out for the B state.

Taken together, our absorption spectra provide evidence that the heme group in resting HRP C is subject to significant in-plane distortions giving rise to a band splitting in the Q- and CT-band region. Moreover, our spectra provide evidence that CT and Q states are electronically coupled, in accordance with suggestions by Zerner and co-workers.<sup>28</sup> With respect to the band assignment we are in agreement with Eaton and Hochstrasser<sup>25</sup> in that physical reasoning leads us to assign the 500 nm band to  $Q_v$  rather than to a second charge-transfer transition. In what follows we now evaluate in detail the distortions of the heme symmetry.

**Decomposition of Raman Spectra.** We used eight wavelengths from our argon laser to measure the polarized spectra of HRP C. All spectra are subjected to the aforementioned global fitting based on previous work of assignment in native HRP<sup>31–33</sup> and  $\text{Ca}^{2+}$ -depleted HRP C.<sup>34</sup> Figure 6 shows the spectra in the region 1280–1700  $\text{cm}^{-1}$  measured with 457.9 and 496.5 nm excitations, which stand for B-band preresonance and  $Q_v$ -band resonance, respectively. A detailed account of the coexisting spin and coordination states, which can be inferred from these spectra, are given in another paper.<sup>34</sup> In the present study, we focus on analyzing the depolarization ratios of four Raman lines, i.e., the oxidation marker ( $\nu_4$ ) at 1373  $\text{cm}^{-1}$  ( $\Gamma = A_{1g}$ ), a band arising from the antisymmetric mode  $\nu_{21}$  at 1310  $\text{cm}^{-1}$ , and the spin marker bands  $\nu_{11}$  and  $\nu_{10c}$  at 1546 and 1635  $\text{cm}^{-1}$  (both  $B_{1g}$ ). Due to their insensitivity to the iron spin state,  $\nu_4$  and  $\nu_{21}$  represent the entire manifold of coexisting spin and coordination states, i.e., hexacoordinated and pentacoordinated high spin (hc-hs and pc-hs) and a third, dominant state that is generally described as quantum mixture between a pentacoordinated intermediate and high spin state (qms: quantum mixed state). The occurrence of pc-qms is a peculiarity of class III peroxi-

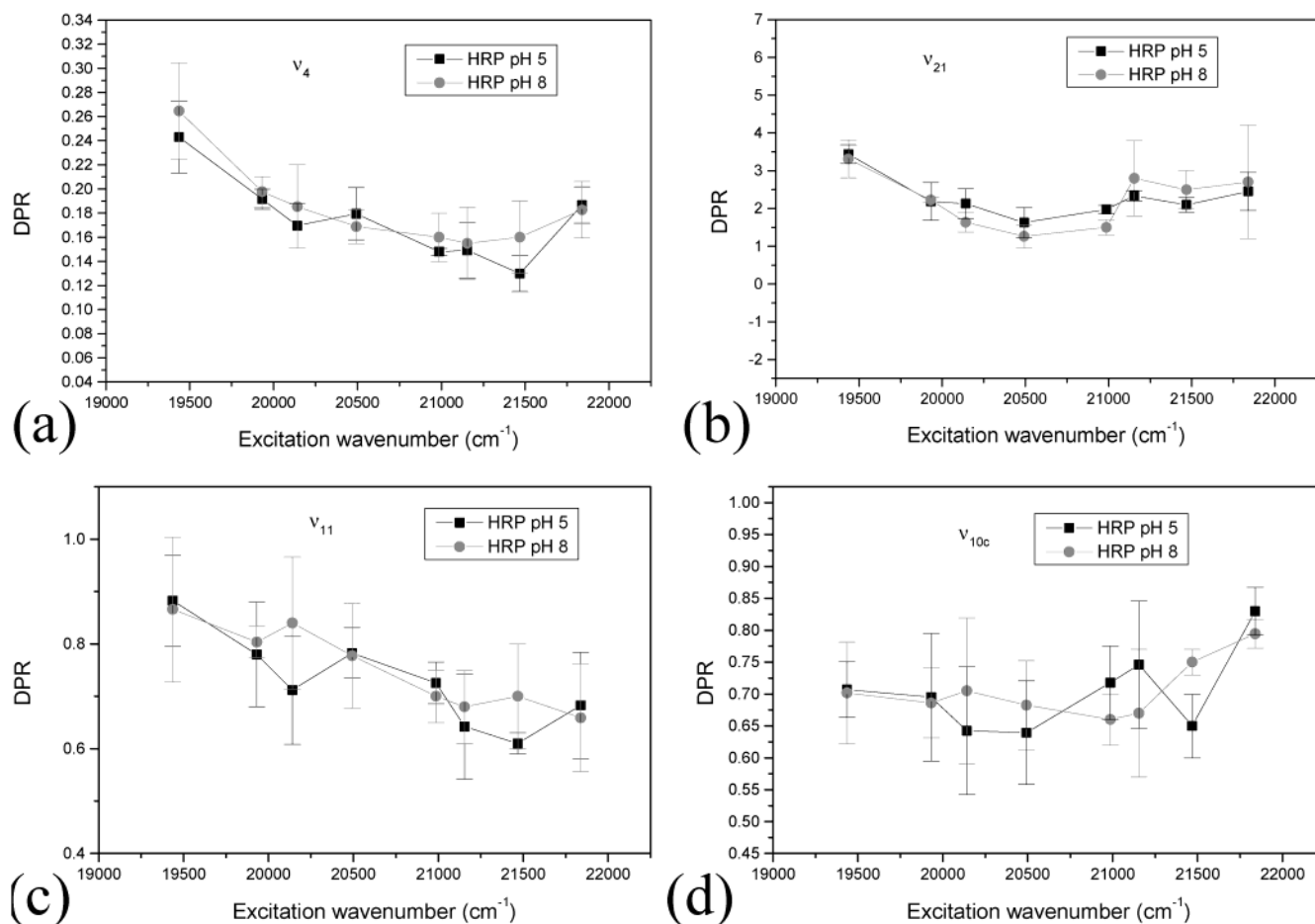


**Figure 7.** DPRs of native HRP at pH 5 and 8 for the Raman modes (a)  $\nu_4$ , (b)  $\nu_{21}$ , (c)  $\nu_{11}$ , and (d)  $\nu_{10c}$ .

dases.<sup>31</sup> Its functional role has yet to be identified, but theoretical evidence suggests that it might facilitate the first step of the enzymatic reaction, i.e., the formation of the compound I heme.<sup>48,49</sup>

**Depolarization Ratio Dispersion of HRP.** Figure 7a–d plots DPRs of native HRP in pH 5.5 and 8.0 for the oxidation marker  $\nu_4$  ( $A_{1g}$  in  $D_{4h}$ ), the spin marker  $\nu_{11}$ ,  $\nu_{10c}$  ( $B_{1g}$  in  $D_{4h}$ ), and  $\nu_{21}$  ( $A_{2g}$  in  $D_{4h}$ ). The DPRs of all four bands show a clear dispersion. For  $\nu_4$ , nearly all values are above 0.125.  $\nu_{11}$  exhibits DPRs below and above its  $D_{4h}$  expectation value 0.75 whereas  $\nu_{10c}$  exhibits most DPRs only below 0.75.  $\nu_{21}$  is apparently inverse and not anomaly polarized.

A qualitative interpretation is easiest for  $\nu_{11}$ . As also demonstrated by the simulations in Figure 3c, DPRs below and above 0.75 reflect the presence of both  $B_{1g}$  and  $B_{2g}$  distortions, respectively.<sup>16,20</sup> Interestingly, the lower DPRs of  $B_{1g}$ -type mode  $\nu_{10c}$  suggest that this mode is only sensitive to  $B_{1g}$  distortion. The reason for this discrepancy between  $\nu_{11}$  and  $\nu_{10c}$  can be inferred from their different normal mode composition.  $\nu_{10}$  contains mainly  $C_m C_\alpha$  stretching, whereas  $\nu_{11}$  is predominantly a  $C_\beta C_\beta$  stretching mode.<sup>19</sup> Hence, the  $B_{2g}$  distortions affecting  $\nu_{11}$  reflect a distortion of the pyrrole rings. This is in agreement with the pattern of the  $B_{2g}$ -type distortion shown in Figure 2. It is thinkable that this distortion results in part from electronic perturbations due to the (unequivalent) vinyl substituents. The lack of influence of  $B_{2g}$  distortions on  $\nu_{10}$  may have two reasons. First,  $\nu_{10}$  is known to have the strongest Jahn–Teller coupling in the Q states, which reduces the dispersion due to  $A_{2g}$  admixture.<sup>16</sup> Second,  $C_m$  cannot contribute to vibronic coupling of  $A_{2g}$  symmetry.<sup>35</sup>

The DPDs of  $\nu_4$  and  $\nu_{21}$  can be explained by  $B_{1g}$  and  $B_{2g}$  distortions as well as by a combination of both. The experimental dispersion is very well comparable with the simulations in Figure 3a,c.  $\nu_4$  is known to be predominantly sensitive to distortions induced by His 170 (Figure 1).<sup>36,37</sup> Corresponding DPRs measured at pH 8 and 5.5 are identical in the limit of accuracy, indicating that the protonation giving rise to the pH dependence of the  $\nu_{Fe-His}$  band<sup>38</sup> has no detectable impact on the heme group in the ferric state. Hence, HRP C behaves like myoglobin in multiple oxidation and spin states, but differently from allosteric proteins such as hemoglobin.<sup>7,39</sup>

It is illuminating to compare our results with the normal-coordinate structural decomposition (NSD) result of native HRP obtained from Shelnett et al. listed in Table 1.<sup>40</sup> The magnitudes of the  $B_{1g}$  and  $B_{2g}$  distortions are remarkably large (0.18 and 0.34 Å, respectively), compared with what was obtained for classical heme proteins such as myoglobin, hemoglobin, and cytochrome *c* (between 0.05 and 0.1 Å).<sup>41</sup> This is in line with the observation that in the region between 457 and 488 nm the depolarization ratios of  $\nu_4$  are systematically higher (0.14–0.19) than those of deoxymyoglobin and myoglobin CN (0.13–0.15)<sup>39</sup> which appear much less distorted in the crystal structure.<sup>41</sup> The dominance of the triclinic  $B_{2g}$  distortion is also peculiar; generally  $B_{1g}$  distortions are larger.<sup>41</sup> This is most likely due to the orientation of the imidazole group of His 170, which is closer to the  $C_m-Fe-C_m$  than to the  $N-Fe-N$  line. The opposite behavior is observed in myoglobin and hemoglobin, where the imidazole group exhibits generally a very small azimuthal angle with respect to the  $N-Fe-N$  line.<sup>42</sup>

The simulation of the DPR dispersion of  $\nu_4$  as described in

the theory section (Figure 3) reveals that the vibronic perturbation energies of the  $B_{1g}$  and  $B_{2g}$  distortions required to account for the observed DPRs are between 30 and 50% of the corresponding coupling energies for  $A_{1g}$  (dot dashed line in Figure 3). This is comparable with observations for myoglobin cyanide for which  $B_{1g}$  distortion in the range of 0.2 Å were obtained from the crystal structure.<sup>37</sup> This suggests that the observed level of  $B_{1g}/B_{2g}$  admixture to the Raman tensor of  $\nu_4$  is at least qualitatively consistent with the distortion values obtained from the NSD analysis of the heme group in the X-ray structure of HRPC.

The structural analysis of Shelnett and associates also reveals out-of-plane distortions, i.e., ruffling (0.99 Å) and saddling (0.87 Å).<sup>11,41</sup> In principle, this gives rise to admixtures of  $A_{2g}$  and  $A_{1g}$  symmetry to  $A_{1g}$  and  $A_{2g}$  modes, respectively. The corresponding vibronic coupling contributions are likely to be weak to be detectable in the spectral region investigated.

How are these distortions related to the band splitting indicated by our optical spectra and observed for Mg-substituted HRP by the fluorescence technique? As outlined in detail by Schweitzer-Stenner and Bigman,<sup>30</sup> one has to consider two contributions to band splitting, namely electronic and vibronic perturbations. With respect to electronic perturbations band splitting is more likely to arise from  $B_{1g}$ -type distortions.  $B_{2g}$  distortions must be strong and concomitant to  $A_{2g}$  distortions to cause any band splitting. We like to emphasize once again that in contrast to what is sometimes indicated in the literature<sup>43</sup> ruffling and saddling, the most prominent out-of-plane distortions in HRP,<sup>11</sup> cannot cause any splitting, because they solely lower the symmetry from  $D_{4h}$  to  $S_4$ . Therefore, only the  $B_{1g}$  perturbations are likely to contribute to the splitting on the electronic level. In principle, the same argument also holds for vibronic perturbations, but as shown by Schweitzer-Stenner and Bigman, additional splitting can be caused by the activation particularly of low-frequency  $E_u$  modes by  $E_u$  distortions of the macrocycle. Such distortions can be induced by a tilted proximal imidazole ring and by a uniform electric field provided by charged residues of the heme environment.<sup>30</sup> The existence of  $E_u$  distortions can be inferred from the existence of bands in the high-frequency region of the Raman spectrum assignable to  $E_u$  modes.

The existence of rhombic distortions is in principle well-known from very early EPR experiments, but for some reason they are generally not discussed in structural terms.<sup>44</sup> However, it is clear from the pattern of the two basic distortions shown in Figure 2, that only the  $B_{1g}$  distortion can be responsible because it involves displacements on the four pyrrole nitrogens that mostly constitute the heme contribution to ligand field. In this context it is of interest to refer to a recent work by Indiani et al.<sup>45</sup> These authors, on the basis of the finding that HRP-BHA exhibits rhombicity and a dominant hc-qms rather state, speculated that the former might be the physical reason for the latter. The possibility of heme distortion causing the qms state had earlier been invoked by Howes et al.,<sup>11</sup> who tried but failed to show any correlation between heme saddling and qms appearance.

Care has to be taken if one discusses the influence of heme perturbations on the electronic states of the central metal. First, one should keep in mind that a pure electronic perturbation associated with a heme distortion cannot mix states of different multiplicities. Second, to analyze the impact of heme perturbations on the electronic structure of the iron atom, it is more appropriate to consider the hierarchy of the d-orbitals. In a tetragonal symmetry and in the presence of a weak axial ligand

the separation between the two higher lying orbitals  $d_{x^2-y^2}$  ( $B_2$ ) and  $d_{z^2}$  ( $A_1$ ) and the lower lying ( $d_{xz}$ ,  $d_{yz}$ ) ( $E_g$ ) and  $d_{xy}$  ( $B_1$ ) is too small to cause a breakdown of Hund's rule so that a high spin state is obtained.<sup>46,47</sup> If the gap increases, the system generally flips to the low spin configuration. An intermediate spin requires a significant increase of the energy gap between  $d_{x^2-y^2}$  ( $B_2$ ) and  $d_{z^2}$  ( $A_1$ ), which would also yield a decrease of the energy between  $d_{z^2}$  ( $A_1$ ) and the lower lying orbitals. This can be accomplished by electronic perturbations of  $B_2(B_{2g})$  symmetry. Thus a  $B_{2g}$  perturbation brings about a stabilization of the intermediate state and concomitantly increases the probability for a mixing between the intermediate and high spin state by decreasing the respective energy difference so that it is shifted into the same order of magnitude as the spin-orbit coupling energy. As mentioned above,  $B_{2g}$  distortions are generally weaker than  $B_{1g}$  distortions in classical heme proteins,<sup>24</sup> so that one is led to the conclusion that it is their extraordinary strength in HRPC that facilitates the spin-orbit coupling, thus giving rise to the qms state. The role of  $B_1(B_{1g})$  perturbations is more difficult to identify. They create a rhombic environment and split the two  $E_g$  orbitals. It is thinkable that this stabilizes the intermediate state further. Ruffling and saddling together create a perturbation of  $A_{2g}(A_2)$  symmetry. In principle it could mix  $B_1(d_{xy})$  and  $B_2(d_{x^2-y^2})$ , but this is unlikely owing to the large energy gap between these orbitals. Hence, the out-of-plane distortions do not facilitate the qms state.

Taken together, our study shows that the heme group of resting HRP C exhibits rhombic distortions along the N-Fe-N ( $B_{1g}$ ) as well as triclinic distortions affecting the  $C_m$ -Fe- $C_m$  distances as well as the pyrrole symmetry ( $B_{2g}$ ). Only the former is responsible for the rhombicity detected in EPR experiments and the optical band splitting observed in this and other studies on HRP derivatives whereas the  $B_{2g}$  distortion facilitates the obtained mixing between intermediate and high spin states of the heme iron. The corresponding electronic perturbation is brought about by the imidazole ring of the proximal histidine, which exhibits a comparatively large azimuthal angle with respect to the N-Fe-N line and nearly eclipses the  $C_m$ -Fe- $C_m$  line. In myoglobin and hemoglobin, the projection of the proximal imidazole shows only a small azimuthal angle (between 0 and 10°) and, as a consequence, the distortion is mostly  $B_{1g}$  rather than  $B_{2g}$ .

**Acknowledgment.** We acknowledge financial support by grants from the National Institutes of Health (COBRE-program P20 RR16439-01) and the Petroleum Research Funds (PRF # 38544-AC4) (R.S.S.), Hungarian OTKA (grant T-032117) (J.F.), and NATO Science Program (ML). We thank Dr. John A. Shelnett for providing us the coordinates for Figure 2. Moreover, R.S.S. and Q.H. thank Dr. Kai Griebenow and Dr. Brad Weiner for allowing them to use their laboratory facilities.

## References and Notes

- (1) Dunford, H. B. In *Peroxidases in Chemistry and Biology*; Everse, J., Everse, K. E., Grisham, M. B., Eds.; CRC Press: Boston, 1991; p 1.
- (2) Tanaka, M.; Ishimori, K.; Mukai, M.; Kitagawa, T.; Morishima, I. *Biochemistry* **1997**, *36*, 9889.
- (3) Howes, B. D.; Rodriguez-Lopez, J. N.; Smith, A. T.; Smulevich, G. *Biochemistry* **1997**, *36*, 1532.
- (4) Ortiz de Montellano, P. R.; Savenkova, M. I. *Arch. Biochem. Biophys.* **1998**, *351*, 286.
- (5) Rodriguez-Lopez, J. N.; Gilabert, M. A.; Tudela, J.; Thorneley, R. N. F.; Garcia-Cánovas, F. *Biochemistry* **2000**, *39*, 13201.
- (6) Ravikanth, M.; Chandrashekar, T. K. *Struct. Bonding (Berlin)* **1995**, *82*, 105
- (7) Schweitzer-Stenner, R. *Quart. Rev. Biophys.* **1989**, *22*, 381.

- (8) Shelnut, J. A. In *The Porphyrin Handbook*; Kadish, K. M., Smith, K. M., Guillard, R., Eds.; Academic Press: San Diego, 2000; Vol. 7, p 167.
- (9) Jentzen, W.; Ma, J.-G.; Shelnut, J. A. *Biophys. J.* **1998**, *74*, 753.
- (10) Ma, J.-G.; Zhang, J.; Franco, R.; Jia, S.-L.; Moura, I.; Moura, J. J. G.; Kroneck, P. M. H.; Shelnut, J. A. *Biochemistry* **1998**, *37*, 12431.
- (11) Howes, B. D.; Schiødt, C. B.; Welinder, K. G.; Marzocchi, M. P.; Ma, J.-G.; Zhang, J.; Shelnut, J. A.; Smulevich, G. *Biophys. J.* **1999**, *77*, 478.
- (12) Kapsoi, A. D.; Wright, W. W.; Fidy, J.; Stavrov, S. S.; Vanderkooi, J. M.; Rasnik, I. *Biochemistry* **2001**, *40*, 3483.
- (13) Kapsoi, A. D.; Vanderkooi, J. M.; Wright, W. W.; Fidy, J.; Stavrov, S. *Biophys. J.* **2001**, *81*, 3472.
- (14) Köhler, M.; Friedrich, J.; Balog, E.; Fidy, J. *Chem. Phys. Lett.* **1997**, *277*, 417.
- (15) Suisalu, A.; Muring, K.; Kikas, J.; Herenyi, L.; Fidy, J. *Biophys. J.* **2001**, *80*, 498.
- (16) Schweitzer-Stenner, R. *J. Porphyrins Phthalocyan* **2001**, *5*, 198.
- (17) McClain, W. M. *J. Chem. Phys.* **1971**, *55*, 2789.
- (18) Unger, E.; Bobinger, U.; Dreybrodt, W.; Schweitzer-Stenner, R. *J. Phys. Chem.* **1993**, *97*, 9956.
- (19) Li, X.-Y.; Czernuszewicz, R. S.; Kincaid, J. R.; Stein, P.; Spiro, T. G. *J. Phys. Chem.* **1990**, *94*, 47.
- (20) Lemke, C.; Dreybrodt, W.; Shelnut, J. A.; Quirke, J. M. E.; Schweitzer-Stenner, R. *J. Raman Spectrosc.* **1998**, *29*, 945.
- (21) Zgierski, M. Z.; Pawlikowski, M. *Chem. Phys.* **1982**, *65*, 335.
- (22) Jentzen, W.; Unger, E.; Karvounis, G.; Shelnut, J. A.; Dreybrodt, W.; Schweitzer-Stenner, R. *J. Phys. Chem.* **1996**, *100*, 14184.
- (23) Dunford, H. In *Heme Peroxidases*; Dunford, H., Ed.; Wiley and Sons: Chichester, U.K., 1999; p 140.
- (24) Schweitzer-Stenner, R.; Cupane, A.; Leone, M.; Lemke, C.; Schott, J.; Dreybrodt, W. *J. Phys. Chem. B* **2000**, *104*, 4754.
- (25) Eaton, W. A.; Hochstrasser, R. M. *J. Chem. Phys.* **1968**, *49*, 985.
- (26) Unger, E.; Dreybrodt, W.; Schweitzer-Stenner, R. *J. Phys. Chem. A* **1997**, *101*, 5997.
- (27) Smulevich, G.; Paoli, M.; de Sanctis, G.; Mantini, A. R.; Ascoli, F.; Coletta, M. *Biochemistry* **1997**, *36*, 640.
- (28) Zerner, M.; Gouterman, M.; Kobayashi, H. *Theor. Chim. Acta* **1966**, *6*, 363.
- (29) Asher, S. A.; Vickery, L. E.; Schuster, T. M.; Sauer, K. *Biochemistry* **1977**, *16*, 5849.
- (30) Schweitzer-Stenner, R.; Bigman, D. *J. Phys. Chem. B* **2001**, *105*, 7064.
- (31) Feis, A.; Howes, B. D.; Indiani, C.; Smulevich, G. *J. Raman Spectrosc.* **1998**, *29*, 933.
- (32) Smulevich, G.; English, A. M.; Mantini, A. R.; Marzocchi, M. P. *Biochemistry* **1991**, *30*, 772.
- (33) Smulevich, G.; Paoli, M.; Burke, J. F.; Sanders, S. A.; Thorneley, R. N. F.; Smith, A. T. *Biochemistry* **1994**, *33*, 7398.
- (34) Huang, Q.; Laberge, M.; Fidy, J.; Schweitzer-Stenner, R. *Biospectroscopy*, in press.
- (35) Gouterman, M. *J. Chem. Phys.* **1959**, *30*, 1139.
- (36) Schweitzer-Stenner, R. *Q. Rev. Biophys.* **1989**, *22*, 381.
- (37) Schweitzer-Stenner, R.; Cupane, A.; Leone, M.; Lemke, J.; Schott, J.; Dreybrodt, W. *J. Phys. Chem. B* **2000**, *104*, 4754.
- (38) Tanaka, M.; Ishimori, K.; Mukai, M.; Kitagawa, T.; Morishima, I. *Biochemistry* **1997**, *36*, 9889.
- (39) El Naggari; Dreybrodt, W.; Schweitzer-Stenner, R. *Eur. Biophys. J.* **1985**, *12*, 43.
- (40) Shelnut, J. A. Personal communication.
- (41) Shelnut, J. A. <http://jasheln.unm.edu>
- (42) Schweitzer-Stenner, R.; Dreybrodt, W. *J. Raman Spectrosc.* **1992**, *23*, 539.
- (43) Rasnik, I.; Sharp, K. A.; Fee, J. A.; Vanderkooi, J. M. *J. Phys. Chem. B* **2001**, *105*, 292.
- (44) Blumberg, W. E.; Peisach, J.; Wittenber, J. B. *J. Biol. Chem.* **1968**, *243*, 1854.
- (45) Indiani, C.; Feis, A.; Howes, B. D.; Marzocchi, M. P.; Smulevich, G. *J. Am. Chem. Soc.* **2000**, *122*, 7368.
- (46) Henriksen, A.; Schuller, D. J.; Meno, K.; Welinder, K. G.; Smith, A. T.; Gajhede, M. *Biochemistry* **1998**, *37*, 8054.
- (47) Harris, G. *J. Chem. Phys.* **1968**, *48*, 2191.
- (48) Maltempo, M. M. *J. Chem. Phys.* **1974**, *61*, 2540.
- (49) Maltempo, M. M.; Ohlsson, P.-I.; Paul, K. G.; Ehrenberg, A. *Biochemistry* **1979**, *18*, 2935.